

Supporting Information

Energy Level Tuning at the MAPbI₃ Perovskite/Contact Interface using Chemical Treatment

Daniele Meggiolaro,^{a,b,*} Edoardo Mosconi,^a Andrew H. Proppe,^{c,d,*} Rafael Quintero-Bermudez,^d

Shana O. Kelley,^{c,e} Edward H. Sargent,^d Filippo De Angelis^{a,f}

^a*Computational Laboratory for Hybrid/Organic Photovoltaics (CLHYO), Istituto CNR di Scienze e
Tecnologie Molecolari (ISTM-CNR), Via Elce di Sotto 8, 06123, Perugia, Italy.*

^b*CompuNet, Istituto Italiano di Tecnologia, Via Morego 30, 16163 Genova, Italy.*

^c*Department of Chemistry, University of Toronto, Toronto, Ontario, Canada, M5S 3G4*

^d*The Edward S. Rogers Department of Electrical and Computer Engineering, University of
Toronto, Toronto, Ontario, Canada, M5S 3G4*

^e*Department of Pharmaceutical Sciences, Leslie Dan Faculty of Pharmacy, University of Toronto,
Toronto, Ontario, Canada, M5S 3M2*

^f*Department of Chemistry, Biology and Biotechnology, University of Perugia, Via Elce di Sotto 8,
06123 Perugia, Italy*

E-mail: daniele.meggiolaro@iit.it (D.M); andrew.proppe@mail.utoronto.ca (A.P.)

Computational details

DFT calculations have been carried out on the (001) MAPbI₃ surface within the supercell approach by using the Perdew-Burke-Ernzerhof (PBE)¹ functional. Slabs models have been built starting from the tetragonal phase of MAPbI₃, by fixing cell parameters to the experimental values.² A 10 Å of vacuum were added along the non-periodic direction perpendicular to the slabs in all cases.

Starting from the flat PbI₂-terminated (001) surface, surface formation energies (SFE) and ionization energies (IE) for increasing numbers of MAI units in the surface layers have been calculated. To this aim, 2x2 in-plane supercells were built starting from the 1x1 MAI-terminated surface by removing MAI units from the external layers until the PbI₂-terminated surface were obtained, i.e. zero MAI-coverage. A symmetric disposition of the organic cations on the external layers of the slabs has been adopted in all cases, leading to supercells with zero average dipole moments. Such arrangement of organic cations provided a flat electrostatic potential in the vacuum region of the supercells for all the modelled slabs.

The stability of surfaces have been estimated by calculating the associated surface formation energies (SFE) by following the equation

$$SFE = \frac{E^S - \sum_i n_i \mu_i}{2A} \quad (1)$$

where E^S is the energy of the modelled slab, n_i and μ_i are the number and the chemical potentials of the species composing the slab, i.e. MA, Pb and I, and A is the area of the slab. Chemical potentials in equation 1 have been fixed to the chemical potentials of the species in the MAPbI₃ bulk in order to guarantee the thermodynamic equilibrium of the surface with the respective bulk phase. Values of the chemical potentials of the bulk species on the other hand have been calculated by imposing equilibrium between MAPbI₃ and PbI₂ bulk phases, i.e. satisfying the following equilibria



Calculated SFEs of slabs at different MAI-coverages were independent from the growth conditions of the perovskite, i.e. the values of the chemical potentials, due to the integer number of MAI and PbI₂ units in the modelled slabs. Calculated SFEs at the PBE level have been corrected by applying dispersions interactions through the DFT-D3 scheme of Grimme³ at the relaxed PBE structures. In selected cases we performed full PBE-D3³ geometry relaxations (see Table S1) obtaining quantities in good agreement with the frozen approach. Notably, SFEs calculated without including dispersion corrections show lower values of SFEs, negative for MAI-rich slabs (see Table S3). Physically correct positive values of SFEs are obtained when dispersions interactions are included.

The energy positions of the valence bands (VBM) in differently terminated surfaces have been quantified by calculating the associated ionization energy (IE). IE is here defined as the energy required to extract electrons from the VB. Notably, this quantity is different from the work function of the slab, defined as the energy required to extract electrons from the Fermi level of the system that is largely influenced by the charge carriers densities and defects at the surface.⁴

IEs have been calculated by using the expression

$$IE = E(vac) - E(VBM) \quad (2)$$

where $E(vac)$ is the potential in the vacuum, i.e. the sum of the pseudo and Hartree potentials ($V_{PS} + V_H$) in the vacuum region between periodic slabs, and $E(VBM)$ is the energy of the top of the valence band of bulk MAPbI₃. The VBM of bulk MAPbI₃ used in Equation 2 were obtained by following an alignment procedure of the electrostatic potential in the slab and in the bulk MAPbI₃. Such approach provides a faster convergence of calculated IEs with the number of inorganic layers in the slab. The calculated IEs without the alignment procedure show a slow convergence vs the number of layers in the slab, while after the alignment procedure they rapidly converge even in 3 layers slabs (see Table S4). IEs at different MAI coverages have been calculated by using the PBE¹ and the hybrid HSE06 functionals⁵, in the last case by including spin-orbit coupling (SOC) and by

using an increased fraction of exact exchange $\alpha=0.43$. Semi-local functionals like PBE, in fact, do not provide an accurate description of the electronic properties of perovskites due to self-interaction error, while the use of hybrid HSE06 functional with an increased fraction of exact exchange $\alpha=0.43$, SOC included, provides an accurate estimate of the electronic properties of MAPbI₃ in agreement with state of the art GW calculations and experiments.^{6,7} In order to evaluate IEs at the HSE06-SOC level we calculated the VBM shift at this level of theory with respect to the PBE functional in bulk MAPbI₃. By using the HSE06-SOC functional a down-shift of the VBM energy of 0.5 eV is obtained with respect to the PBE calculation, in agreement with previous calculations.⁷ The down-shift of the VBM found at the hybrid SOC level for bulk MAPbI₃ has been thus rigidly applied to the IE values calculated at the PBE level in order to obtain HSE06-SOC values in Table S1.

Convergence tests on the calculated SFEs and IEs vs the number of Pb-I inorganic layers in the slab have been carried out in the 1x1 MAI-terminated surface (see Table S4). The calculated band gaps show a slow convergence with the number of layers in the slab. For the MAI-terminated surface the calculated band gaps approach the bulk value limit by including 11 inorganic layers in the slab (see Table S4).

SFEs and IEs of slabs at different MAI coverages have been calculated in the 2x2 in-plane surfaces with 5 Pb-I inorganic layers, by sampling the BZ at the Γ point only. The impact of supercell size and k-points sampling on the accuracy of the calculated quantities have been also investigated by comparing SFEs, band gaps and IEs for differently terminated (001) surfaces in the 1x1 and 2x2 slabs and for different k-points sampling in the BZ. Results are summarized in Table S5. Results reported in Table S5 highlight a fairly good convergence of the calculated quantities in the 2x2 slabs with a Γ -only k-point sampling.

PBE surface calculations have been performed by using ultrasoft pseudopotentials (shells explicitly included in calculations: I 5s, 5p; N, C 2s, 2p; O 2s 2p; H 1s; Pb 6s, 6p, 5d) and a

cutoff on the wavenfunctions of 40 Ryd (320 Ryd on the charge density). Hybrid HSE06-SOC calculation on the unit cell of bulk MAPbI₃ has been carried out by using norm-conserving pseudopotentials (shells explicitly included in calculations: I 5s, 5p; N, C 2s, 2p; H 1s; Pb 5s, 5p, 5d, 6s, 6p) with an energy cutoff on the wavefunctions of 40 Ryd and a 2x2x2 k-points grid in the BZ. All calculations were performed by using the Quantum Espresso package.⁸

Projected density of states (DOS) reported in diagrams of Figure 1d-f in the main text have been calculated at the PBE level following the approach already used in our previous work⁹ and represent slab's projected DOS as a function of the energy (x axis) and of the z-coordinate orthogonal to the slab surface. For a direct comparison the calculated DOS reported in the diagrams have been aligned to vacuum level in all cases.

Experimental details

Photoluminescence

Photoluminescence (PL) measurements were performed using a Horiba Fluorolog Time Correlated Single Photon Counting (TCSPC) system with photomultiplier tube detectors. A pulsed laser diode (Horiba, DD-510L) with a peak wavelength of 508 nm and a pulse width of 110–140 ps was used as the excitation source for transient measurements. A 400 ns period was used to capture accurate carrier lifetimes, resulting in a pulse energy of 0.56 nJ.

X-ray photoelectron spectroscopy (XPS) and Ultraviolet photoelectron spectroscopy (UPS)

XPS and UPS measurements were carried out in an Escalab Xi+ Microprobe system. The XPS measurements were carried out with an Al K α source with a spot size of 900 μ m and energy steps of 0.05 eV. The ultraviolet photoelectron spectroscopy measurements were carried out with a He 1 α source with a spot size of 2.5 mm and energy steps of 0.02 eV. Perovskite thin films were spin coated onto plasma-treated ITO substrates, and a corner of the film was scratched off where electrically-conductive carbon tape was adhered to avoid charging. All UPS measurements were

conducted with a 5 V bias. The ultraviolet photoelectron spectroscopy measurements were carried out first followed by the XPS measurements within the same pump-down so as to avoid sample damage by the latter on the former more surface-sensitive measurement.

Table S1. Surface formation energies (PBE-D3), band gaps (PBE) and Ionization Energies (HSE06-SOC, $\alpha=0.43$) calculated for different MAI-coverage θ of the (001) surface. D3 dispersion corrections have been applied a-posteriori on the relaxed PBE structures. In parenthesis quantities calculated performing full PBE-D3 relaxation procedures have been reported. Surfaces with $\theta=0$, 0.5 and 1.0 have been labelled as A, B, C, respectively. Their structures are reported in Figure 1 of the main text.

MAI coverage (θ)	SFE – PBE D3 (eV/nm²)	E_{gap} - PBE (eV)	IE – HSE06-SOC (eV)
0.000 (A)	1.59 (1.44)	1.43 (1.43)	6.38 (6.31)
0.125	1.50	1.51	6.08
0.250	1.46	1.62	5.77
0.375	1.27	1.69	5.53
0.500 (B)	1.14 (0.99)	1.72 (1.68)	5.29 (5.50)
0.625	0.91	1.74	5.07
0.750	0.74	1.77	4.86
0.875	0.48	1.78	4.76
1.000 (C)	0.20 (0.11)	1.85 (1.87)	4.68 (4.94)
H ₂ O @ (A, $\theta=0$)		1.86 (1.87)	5.67 (5.74)

Table S2. Average chemical composition of the surfaces for different treatment of the MAPbI₃ film and associated VBM measured by UPS.

Chemical treatment of the surface	Composition of the surface	VBM (eV)
PbI ₂ treatment	~10% more PbI ₂ surfaces	5.8
No treatment (control)	~1:1 MAI and PbI ₂ surfaces	5.7
MAI treatment	Similar to control	5.1
	~20% more MAI-surfaces	4.7
	~50% more MAI-surfaces	4.4

Table S3. Calculated surface formation energies (SFE) without (wo) and with D3 dispersions corrections, band gap (E_{gap}) at the PBE level and Ionization Energies (IE) at the PBE / HSE06 (SOC) levels of theory for the modelled slabs at different MAI coverage of the (001) surface. All calculations have been performed in the 2x2 supercell at the Γ point by using ultrasoft pseudopotentials with a cutoff on the wavefunctions of 40 Ryd (320 Ryd on the charge density). D3 corrections on the SFEs have been applied by performing single point PBE-D3 calculations on the relaxed PBE structures.

MAI coverage (θ)	SFE PBE wo / with D3 (eV/nm ²)	E_{gap} PBE (eV)	IE PBE / HSE06-SOC (eV)
------------------------------	--	---------------------------------	-------------------------------

0.000 (A)	0.68 / 1.59	1.43	5.88 / 6.38
0.125	0.56 / 1.50	1.51	5.58 / 6.08
0.250	0.48 / 1.46	1.62	5.27 / 5.77
0.375	0.30 / 1.27	1.69	5.03 / 5.53
0.500 (B)	0.19 / 1.14	1.72	4.79 / 5.29
0.625	0.00 / 0.91	1.74	4.57 / 5.07
0.750	-0.14 / 0.74	1.77	4.36 / 4.86
0.875	-0.34 / 0.48	1.78	4.26 / 4.76
1.000 (C)	-0.55 / 0.20	1.85	4.18 / 4.68

Table S4. Calculated SFEs, band gaps and IEs vs number of layers in the 1x1 slab of the MAI-terminated surface at the PBE level. SFE have been calculated by performing PBE-D3³ single point calculations on the relaxed PBE structures, while in parenthesis values calculated by performing full PBE-D3 relaxations have been reported. IE values calculated with and without alignment procedure with the bulk electrostatic potentials have been reported. Calculations have been performed by using ultrasoft pseudopotentials with a cutoff on the wavefunctions of 40 Ryd (320 Ryd on the charge density) and 2x2x1 grids of k-points in the BZ.

Pb-I layers	SFE (eV/nm²)	E_{gap} (eV)	IE/wo align (eV)	IE/w align (eV)
3	0.22 (0.15)	1.99	4.70	4.24
5	0.20 (0.15)	1.85	4.67	4.24
7	0.22 (0.10)	1.71	4.60	4.23
11	0.22 (0.12)	1.64	4.54	4.22
bulk		1.59		

Table S5. Convergence tests on the supercells size and the k-point sampling for calculated SFEs, E_{gap} and IE in the 5-layers slabs. SFEs have been calculated by performing single points PBE-D3 on the PBE relaxed structures.

	1x1 sc (4x4x1 k points)	1x1 sc (2x2x1 k points)	2x2 sc (Gamma)
SFE (eV/nm²)			
PbI ₂ -term	1.48	1.59	1.59
MAI-term	0.09	0.20	0.20
E_{gap} (eV)			
PbI ₂ -term	1.37	1.39	1.43
MAI-term	1.83	1.85	1.85
IE (eV) - PBE			
PbI ₂ -term	5.86	5.91	5.88
MAI-term	4.27	4.24	4.18

Table S6. Elemental ratios on surface of untreated and MAI-treated MAPbI₃ determined from XPS.

Values for I, C and N are normalized relative to Pb.

Sample	Pb	I	C	N
MAPbI ₃ (untreated)	1	4.7	3.2	1.5
+1 mgmL ⁻¹ MAI	1	4.23	4.5	1.4

+3 mgmL ⁻¹ MAI	1	5	4.1	1.7
+5 mgmL ⁻¹ MAI	1	4.8	3.5	2.2

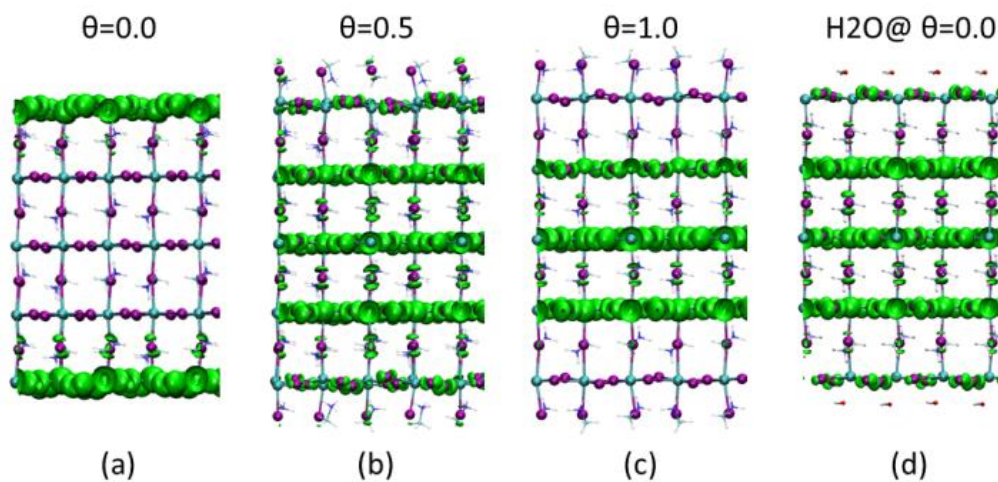


Figure S1. Plot of the HOMO orbitals of the (001) surfaces of MAPI for different MAI coverages, i.e. $\theta=0.0, 0.5, 1.0$, and for the PbI₂ terminated surface with adsorbed water molecules (adsorbed water molecules bind lead ions on the surface at distance of ~ 2.6 Å). Isosurface values used for plots were the same in all cases (10^{-4}).

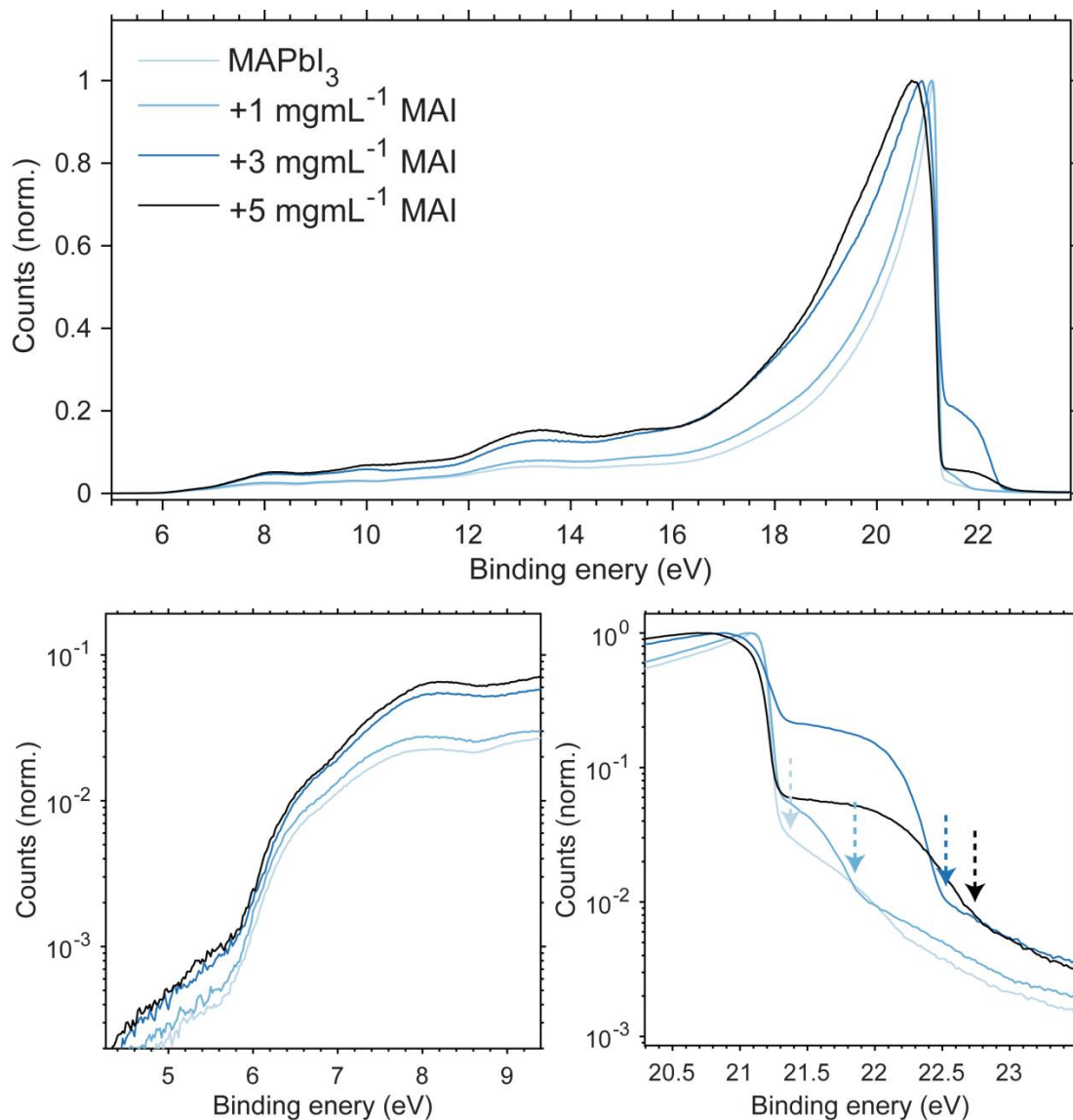


Figure S2. Ultraviolet Photoelectron spectra for MAI-treated MAPbI₃ films. (left) Full spectra and (right) close up view of the onset region of the spectra. As discussed in the main text, the low kinetic energy (high binding energy) part of the spectrum contains two discernible photoemission intensity drop-offs (indicated by arrows for each different film). This would suggest that the film consists of both band-shifted and un-shifted components. This might be attributed to the limitations of the MAI-treatment, which may only be successful in parts of the film with exposed PbI₂ facets. For clarity in this figure, the spectra were shifted such that the larger, ‘unshifted’ drop-off in the high binding energy region intercepted the noise floor at 21.2 eV. The shifted spectra then represent binding energy (with respect to the vacuum level) for the un-shifted components. To analyse the band-shifted components, the secondary drop-off in the high binding energy region was used

instead, effectively shifting the photoemission spectra towards lower binding energy values. The intercept of the photoemission onset with the noise floor in the low binding energy region was taken to be the VBM.

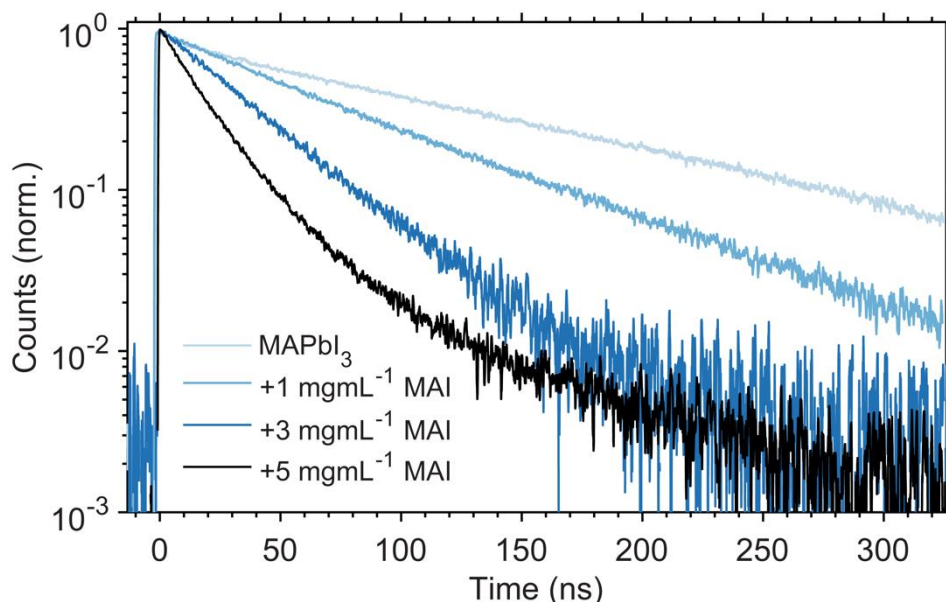


Figure S3. Photoluminescence lifetimes for MAI-treated MAPbI₃ films without quencher layer (no spiro-OMeTAD). Film deposition and PL measurements were carried out under identical conditions as the MAPbI₃/Spiro experiments.

References:

- (1) Perdew, J. P.; Burke, K.; Ernzerhof, M. Generalized Gradient Approximation Made Simple. *Phys. Rev. Lett.* **1996**, *77*, 3865-3868.
- (2) Stoumpos, C. C.; Malliakas, C. D.; Kanatzidis, M. G. Semiconducting Tin and Lead Iodide Perovskites with Organic Cations: Phase Transitions, High Mobilities, and near-Infrared Photoluminescent Properties. *Inorg. Chem.* **2013**, *52*, 9019-9038.
- (3) Grimme, S.; Antony, J.; Ehrlich, S.; Krieg, H. A Consistent and Accurate Ab Initio Parametrization of Density Functional Dispersion Correction (Dft-D) for the 94 Elements H-Pu. *J. Chem. Phys.* **2010**, *132*, 154104.

- (4) Kahn, A. Fermi Level, Work Function and Vacuum Level. *Materials Horizons* **2016**, 3, 7-10.
- (5) Heyd, J.; Scuseria, G. E.; Ernzerhof, M. Hybrid Functionals Based on a Screened Coulomb Potential. *J. Chem. Phys.* **2003**, 118, 8207-8215.
- (6) Umari, P.; Mosconi, E.; De Angelis, F. Relativistic Gw Calculations on $\text{CH}_3\text{NH}_3\text{PbI}_3$ and $\text{CH}_3\text{NH}_3\text{SnI}_3$ Perovskites for Solar Cell Applications. *Sci. Rep.* **2014**, 4, 4467.
- (7) Meggiolaro, D.; De Angelis, F. First-Principles Modeling of Defects in Lead Halide Perovskites: Best Practices and Open Issues. *ACS Energy Lett.* **2018**, 3, 2206-2222.
- (8) Giannozzi, P.; Baroni, S.; Bonini, N.; Calandra, M.; Car, R.; Cavazzoni, C.; Ceresoli, D.; Chiarotti, G. L.; Cococcioni, M.; Dabo, I., et al. Quantum Espresso: A Modular and Open-Source Software Project for Quantum Simulations of Materials. *Journal of Physics: Condensed Matter* **2009**, 21, 395502.
- (9) Colella, S.; Mosconi, E.; Pellegrino, G.; Alberti, A.; Guerra, V. L. P.; Masi, S.; Listorti, A.; Rizzo, A.; Condorelli, G. G.; De Angelis, F., et al. Elusive Presence of Chloride in Mixed Halide Perovskite Solar Cells. *J. Phys. Chem. Lett.* **2014**, 5, 3532-3538.